Solution Structure and Backbone Dynamics of the N-Terminal Region of the Calcium Regulatory Domain from Soybean Calcium-Dependent Protein Kinase α†

Aalim M. Weljie,‡ Stéphane M. Gagné,§ and Hans J. Vogel*,‡

Structural Biology Research Group, Department of Biological Sciences, University of Calgary, 2500 University Drive NW, Calgary, Alberta, Canada T2N 1N4, and Département de biochimie et de microbiologie, Pavillon Charles-Eugène-Marchand, Université Laval, Québec, Canada G1K 7P4

Received June 16, 2004; Revised Manuscript Received August 25, 2004

ABSTRACT: Ca^{2+}-dependent protein kinases (CDPKs) are vital Ca^{2+}-signaling proteins in plants and protists which have both a kinase domain and a self-contained calcium regulatory calmodulin-like domain (CLD). Despite being very similar to CaM (>40% identity) and sharing the same fold, recent biochemical and structural evidence suggests that the behavior of CLD is distinct from its namesake, calmodulin. In this study, NMR spectroscopy is employed to examine the structure and backbone dynamics of a 168 amino acid Ca^{2+}-saturated construct of the CLD (NtH-CLD) in which almost the entire C-terminal domain is exchange broadened and not visible in the NMR spectra. Structural characterization of the N-terminal domain indicates that the first Ca^{2+}-binding loop is significantly more open than in a recently reported structure of the CLD complexed with a putative intramolecular binding region (JD) in the CDPK. Backbone dynamics suggest that parts of the third helix exhibit unusually high mobility, and significant exchange, consistent with previous findings that this helix interacts with the C-terminal domain. Dynamics data also show that the "tether" region, consisting of the first 11 amino acids of CLD, is highly mobile and these residues exhibit distinctive β-type secondary structure, which may help to position the JD and CLD. Finally, the unusual global dynamic behavior of the protein is rationalized on the basis of possible interdomain rearrangements and the highly variable environments of the C- and N-terminal domains.

Plant cells are highly dependent on the accurate decoding of Ca^{2+} signals to respond to a variety of stress and metabolic conditions (*1*). The intricate protein machinery involved in the Ca^{2+} response includes not only the ubiquitous calmodulin (CaM)[1] secondary messenger protein but also unique Ca^{2+}-dependent, CaM-independent enzymes, the calcium-dependent protein kinases, also known as the calmodulin-like domain protein kinases (CDPK) (*2*). CDPKs have been shown to be crucial signaling agents in both plants and protists (*3*, *4*) but are not found in yeasts or animals.

The structural bases for the calcium-dependent regulatory functions of CDPK are centered in a Ca^{2+}-binding region (the CaM-like domain, or CLD), with homology to CaM (>40% amino acid sequence identity), located at the C-terminal end of the protein (Figure 1). The sequence homology of the CLD and soybean CDPK-α has been explored through sequence alignments and homology modeling in previous studies (*2*, *5*). The first part of CDPK consists of an N-terminal tail sequence, which is not conserved across species, and a kinase domain with homology to mammalian CaM-dependent kinases. Between the kinase and calcium regulatory regions sits a junction domain (JD), which serves as both an autoinhibitory domain to the kinase (*6*, *7*) and a binding region for the CLD (*8*, *9*).

Significant strides have been made recently in our understanding of the role of the calcium-binding regions based on work from *Arabidopsis* isoform CPK-1 (*10*) and soybean CDPK-α (*11*). The former study (*10*) demonstrates that a 11-residue segment, nicknamed the "tether" region (residues A329−G340) and located immediately downstream of the JD in the N-terminal portion of the CLD, is crucial in intramolecular binding. This same tether region, however, is not required for intermolecular binding of the CLD to the JD (*10*) in experiments where isolated CLD protein and synthetic JD peptide were mixed. The NMR structure and chemical shift evidence from soybean CDPK-α indicates that this result is due to a structural rearrangement of the C-terminal portion of the CLD (residues 413−474) on binding the JD and that the N-terminal lobe (residues 339−403) acts primarily as a structural scaffold which allows this interaction to take place (*11*). Yet the N-terminal lobe is not a passive entity in activation, as evidenced by the sensitivity of *Plasmodium* CDPK enzyme activity to mutation of the Ca^{2+}-binding loops (*12*).

† This work was supported by an operating grant from the National Sciences and Engineering Research Council. H.J.V. holds a Senior Scientist Award from the Alberta Heritage Foundation for Medical Research (AHFMR), while A.M.W. was the recipient of an AHFMR Studentship award.

* Corresponding author: (403) 220-6006 (phone); (403) 289-9311 (fax); vogel@ucalgary.ca (e-mail).

‡ University of Calgary.

§ Université Laval.

[1] Abbreviations: CDPK, calcium-dependent protein kinase; CLD, calmodulin-like domain or calcium-regulatory domain; NtH-CLD, N-terminal lobe of CLD with amino His tag; CaM, calmodulin; JD, junction domain; HSQC, heteronuclear single-quantum coherence; NMR, nuclear magnetic resonance; NOE, nuclear Overhauser effect; NOESY, NOE spectroscopy; CPMG, Carr−Purcell−Meiboom−Gill; TOCSY, total correlation spectroscopy; T_1, longitudinal relaxation time; T_2, transverse relaxation time.

10.1021/bi048751r CCC: $27.50
Published on Web 11/10/2004

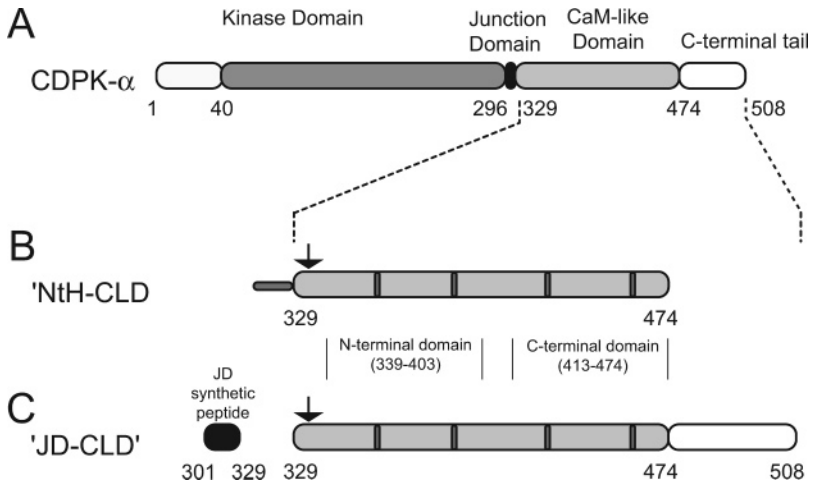

FIGURE 1: Primary structure of (A) soybean CDPK-α, (B) NtH-CLD, and (C) the intermolecular complex of the JD with intact CLD (*11*). The region between 1 and 40 in (A) is the N-terminal tail, which is highly variable between CDPKs from different species. The region indicated prior to residue 329 in (B) is the N-terminal His tag in the position typically occupied by the junction domain. The arrows in (B) and (C) indicate the tether region, between residues A329 and G340, which connects the junction domain and CLD in CDPK. The four dark, vertical areas in (B) and (C) indicate the positions of Gly residues in the four helix−loop−helix Ca^{2+}-binding loops. The positions of the two lobes of the CLD are indicated between (B) and (C), with the region between the two lobes designated as the linker region.

To better understand the structure and dynamics of the N-terminal lobe of the CLD, in this study a unique CLD construct is examined, termed NtH-CLD (Figure 1B), in which almost the entire linker region and C-terminal lobe (residues 404−474) are exchange broadened when examined by NMR in a Ca^{2+}-saturated state. Diffusion analysis (*13*) and fluorescence resonance energy transfer studies (*14*) clearly indicate that the two lobes in the Ca^{2+}-regulatory region of soybean CDPK-α are not independent in the Ca^{2+} form. Hence having both the N-terminal lobe and C-terminal lobe attached is important and allows us to undertake a detailed examination of the N-terminal lobe while maintaining important global structural characteristics.

The major goal of this report is to advance our understanding of the role of the N-terminal lobe in the NtH-CLD, given the highly dynamic nature of the interaction between the N- and C-terminal lobes in this construct. In the first part of this study, we solve the solution structure of the N-terminal lobe of CLD by NMR spectroscopy, which proves to be somewhat distinct from the previously reported structure of CLD with a peptide encompassing the JD (*11*). The second part of this examination entails characterization of the backbone dynamic properties of the N-terminal lobe. Finally, the presence of significant exchange in many parts of the N-terminal lobe is described, and special emphasis is laid on the biological consequence with respect to the implication of interdomain motions in CLD and related proteins.

MATERIALS AND METHODS

Protein Expression and Purification. The CLD cDNA from soybean CDPK-α (residues A329−K508) was generously provided by Dr. A. C. Harmon (University of Florida). The region of the CLD gene with homology to CaM (A329−K472) was PCR amplified out of the original pET-3b construct and cloned into the pET-19b vector (Novagen) to give the "NtH-CLD" gene. This step eliminated the C-terminal tail, thought to be proteolytically cleaved during expression (*8*), and added a 23-residue N-terminal sequence ((*M*)G-H_{10}-SSGHIDDDDKHM). Briefly, protein was expressed in *Escherichia coli* BL21(DE3), with ^{15}N-NtH-CLD and ^{15}N/^{13}C-NtH-CLD expressed in MOPS-based minimal medium (*15*) with 10 g/L unlabeled glucose and 3 g/L ^{13}C-labeled glucose (CIL), respectively. Purification was achieved essentially as described previously using an initial Ni^{2+} affinity column and subsequently Ca^{2+}-dependent hydrophobic chromotography (*11*). Purity was >98% as assessed by Coomassie blue stained SDS−PAGE. Buffer exchange into a 5 mM ammonium bicarbonate solution was accomplished using a PD-10 column (Bio-Rad), and subsequently protein samples were lyophilized and stored at −20 °C prior to use in NMR experiments.

NMR Spectroscopy. Samples for NMR experiments were prepared in a bufferless 90/10% H_2O/D_2O solution, 200 mM KCl, 10 mM $CaCl_2$, and 1 mM DTT, pH 6.1. The pH was adjusted with KOD and DCl, and the final pH was not adjusted for isotope effects. The ^{15}N-NtH-CLD sample was 0.55 mM protein in 400 μL, and the ^{15}N/^{13}C-NtH-CLD sample was ∼0.8 mM in protein in 600 μL. ^{1}H/^{15}N/^{13}C backbone resonance assignments were accomplished with sensitivity-enhanced versions (*16*) of CBCA(CO)NH (*17*)/CBCANH (*18*) and HNCO (*16*)/HN(CA)CO (*19*) experiments on a 800 MHz Varian Inova spectrometer (NANUC, University of Alberta). A 3D ^{15}N-edited NOESY spectrum (*20*) was also acquired at 800 MHz on the ^{15}N-NtH-CLD sample with a mixing time of 150 ms. Previously reported NMR assignments from a JD-CLD complex (*11*) (CLD construct of Figure 1C), as well as H(CC)(CO)NH, (H)CC-(CO)NH (*21*), and HBHA(CO)NH (*22*), were used to obtain side chain assignments. All side chain experiments were conducted at 500 MHz on a Bruker DRX spectrometer equipped with a triple resonance 5 mm TXI cryoprobe with a *z*-axis gradient channel. All spectra were acquired at 303 K and referenced with respect to a ^{1}H chemical shift of 0 ppm for the most upfield resonance of 5,5-dimethylsilapentanesulfonate (DSS) (*23*). Data were processed with NMRPipe 2.1 (*24*) and analyzed with NMRView 5.0.3 (*25*).

Structure Determination. Structural NOE data for the NtH-CLD-protein were extracted from the ^{15}N-edited NOESY at 800 MHz. ARIA 1.2/CNS 1.1 was used for all structure calculations (*26*, *27*). Dihedral angle restraints were derived

using both CSI (*28*) and TALOS (*29*) based analysis of the chemical shifts. Non-glycine residues with no CSI or TALOS data were subject to ϕ dihedral angle restraints of $-35°$ to $-175°$ based on accepted geometry to accelerate structural convergence in the initial stages of structural calculations. Eight of these residues were within the range of residues showing secondary structure; however, these restraints had an insignificant impact on the final data. Additional restraints of 2.40 ± 0.40 Å were introduced in the calcium-binding loops for coordinating protein oxygen atoms to Ca^{2+} ions based on the well-established EF-hand metal-binding motif (*30*). The simulated annealing protocol was initiated from a fully extended conformation. In the final two iterations, 50 and then 200 structures were calculated, and the lowest energy 15 were selected for the final structure ensemble. The final ensemble was evaluated using AQUA 3.2 and PROCHECK 3.5 (*31*).

Backbone Relaxation. ^{15}N T_1, T_2, and $\{^1H\}-^{15}N$ NOE data were acquired at 500 MHz using 2D-HSQC-type experiments. Longitudinal delays of 5, 65, 145, 246, 366, 527, and 757 ms (T_1) and CPMG delays of 8.4, 25,1, 41.8, 58.6, 75.3, 108.8, 125.0, and 142.3 ms (T_2) were used in acquisition of ^{15}N,^1H correlated spectra (*32*). To minimize the effects of heating in the T_2 experiments, a recycle delay of 2 s was used, as were dummy CPMG pulses. Steady-state heteronuclear $\{^1H\}-^{15}N$ NOE data were obtained with and without 3 s of proton saturation and a total recycle delay of 5 s, and subsequently NOE values were extracted as the ratio of peak volumes with and without proton saturation (*32*). All spectra were acquired using standard Bruker pulse programs which incorporate sensitivity enhancement (*32*) and water flip-back pulses (*33*). Acquisition size was 2K × 128 points at 500 MHz. Spectra were linear predicted, zero-filled, and baseline corrected in the indirectly detected dimension, and zero-filled in the directly detected dimension. Analysis of T_1 and T_2 decay rates was accomplished via the rate analysis functions in NMRView using peak volume integration to minimize errors (*34*), and a noise floor of 3%, 4%, and 7% was used in calculation of T_1, T_2, and $\{^1H\}-^{15}N$ NOE, respectively.

Initial estimates of the global tumbling parameters were obtained using Modelfree 4.15 (*35, 36*), after excluding residues which had NOE values <0.65. The method of Tjandra et al. (*37*) to account for conformational exchange was not successful in estimating the correlation time, presumably due to the presence of an excessive amount of exchange in all residues. As a result, an alternative strategy for initial estimates of τ_m was employed whereby an S^2-R_{ex} model was used and the exchange constant was allowed to vary by one-half of the T_2 value. Subsequent analysis of relaxation data was conducted using the extended model-free formalism of Lipari and Szabo (*38*, *39*), using the statistical approach of Mandel et al. (*35*). Values for the ^{15}N gyromagnetic ratio, bond length, and chemical shift anisotropy were -2.71 T^{-1} $s^{-1}/10^7$, 1.02 Å, and -172 ppm, respectively.

RESULTS

In the initial stages of working with the NtH-CLD construct, the protein behaved very similarly to that in previously reported work (*5*, *11*). A high degree of purity was achieved by initial Ni^{2+} affinity chromatography followed by Ca^{2+}-dependent hydrophobic chromatography, as judged by SDS−PAGE (not shown). Fluorescence resonance energy transfer experiments also suggested a significant change in the overall structure of the protein (Robertson, Weljie, and Vogel, unpublished observations) similar to that observed with the CLD construct (*14*) of Figure 1C. As a result,^{15}N-labeling of the protein was undertaken for NMR structure determination of the Ca^{2+}-saturated form of NtH-CLD. Initial ^1H,^{15}N-HSQC spectra of ^{15}N-NtH-CLD suggested a large degree of chemical exchange, with significant attenuation of numerous peak intensities, as well as fewer than the expected 166 peaks present (Figure 2). Preliminary analysis of the ^{15}N-edited NOESY spectrum suggested that the intense peaks were in a well-folded region with numerous NOE's evident, and thus ^{15}N/^{13}C-labeled protein was also prepared for assignment of this region.

C-Terminal Domain Exchange. In the course of analyzing assignment datasets it became clear that the well-folded, non-exchange-broadened region of NtH-CLD was primarily the N-terminal Ca^{2+}-binding region. Nearly complete backbone (HN, N, CA, HA, CO) and side chain (CB, HB, and side chain protons) assignments were obtained for the tether region (A329−G340), as well as the remainder of the N-terminal domain of NtH-CLD up to A399. Two other short stretches were assigned in the C-terminal domain, four residues in the third Ca^{2+}-binding region (D422−G425) and the five C-terminal residues (A468−K472). In addition, three Gly resonances were immediately evident between 10.5 and 11.2 ppm, highly characteristic of helix−loop−helix Ca^{2+}-binding proteins, assigned to be from the first three Ca^{2+}-binding loops (G353, G389, and G425). Interestingly, no assignable resonances from the fourth Ca^{2+}-binding region were found (Figure 2), although a broad peak near the level of noise near 9.6 ppm (^1H)/112.6 ppm (^{15}N) is proposed to be the G459 from the fourth Ca^{2+}-binding loop. Taken together, this provided a nearly complete assignment of the HSQC, although some intense peaks remained unassigned (Figure 2). Analysis of the assignments using the Chemical Shift Index (*28*, *40*) suggested that the secondary structure of the N-terminal domain was a dual helix−loop−helix repeat as expected for an EF-hand Ca^{2+}-binding protein.

As we were perplexed by the absence of peaks from the C-terminal domain, a series of different pHs (6.1, 6.5, 7.0, 7.5) and temperatures (25, 30, 35, 40 °C) were tested in an attempt to find conditions in which the C-terminal domain was assignable. The pH titrations had little effect, but interestingly the temperature titrations elucidated an intriguing effect (Figure 3). At 40 °C the protein clearly maintains its fold (Figure 2), and a number of unassigned peaks that were very weak at 25 °C became quite intense, while several new peaks appeared. Generally, the peak intensities of the N-terminal domain peaks increased by about 100−200% between 25 and 40 °C. On the other hand, the peak intensity increase for the C-terminal domain residues was generally between 300% and 500%, clearly indicating that the behavior of the two lobes of the protein was distinct. Residues from terminal and predicted loop regions show the smallest increases and even some decreases, probably due to increased exchange with dephased water protons at higher temperature. Regions with predicted helical structure show an increase in peak intensity, presumably due to decreased rotational correlation time of the molecule promoting sharper NMR

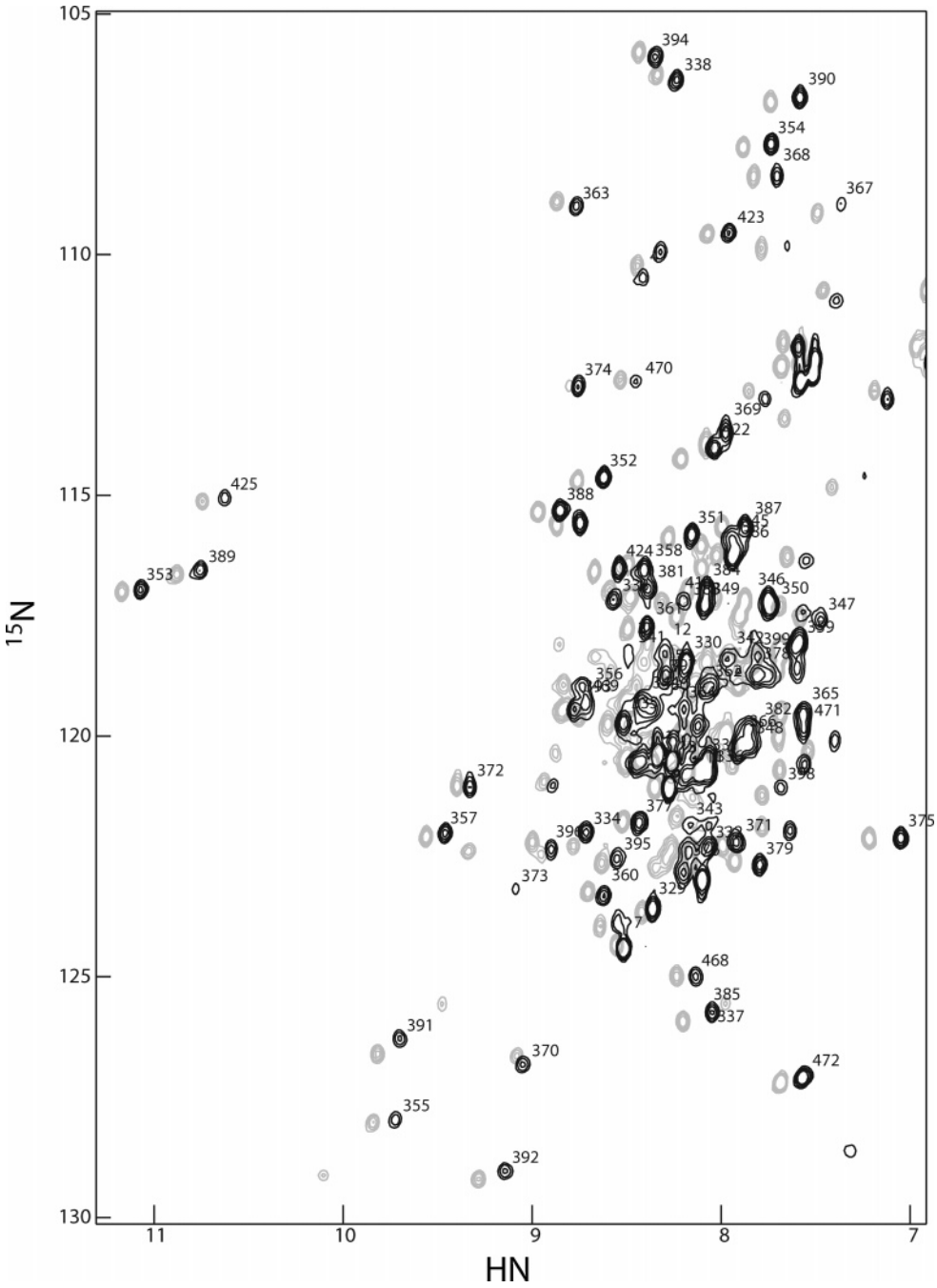

FIGURE 2: Temperature dependence of peaks from the ^{1}H,^{15}N-HSQC of NtH-CLD, acquired at 25 °C (dark) and 40 °C (light). In addition to movement of the chemical shift with increasing temperature, the intensity of the peaks generally also increases, although in this case the increase was not uniform between N-terminal and C-terminal residues. The presence of G425 near 10.5 ppm but the absence of G459 suggests that it is the fourth calcium-binding loop which is involved in an exchange phenomenon, although it appears to affect the entire C-terminus.

line widths. The increase due to faster tumbling will be equally applicable to both N-terminal and C-terminal domains; hence the C-terminus must also be undergoing some other type of exchange to account for the significant difference. Unfortunately, the protein was prone to precipitation and degradation at higher temperatures (data not shown); thus further experiments at 40 °C could not be conducted, and the remainder of the structural analysis was limited to the N-terminal region. In addition, acquiring spectra at 500 MHz (not shown) did not significantly alter the observed ^{1}H,^{15}N-HSQC spectrum compared to 800 MHz.

NtH-CLD Structure. Superposition of the 15 lowest energy structures consistent with the NOE and dihedral angle constraints is presented in Figure 4A, and the structural statistics for the ensemble are presented in Table 1. A total of 883 NOE-derived distance restraints were used, of which 765 were unambiguous, and a total of 130 dihedral restraints. The structure is characterized by a disordered N-terminus (which includes a portion of the N-terminal His tag) and a reasonably well-ordered core region. Typical of EF-hand Ca^{2+}-binding proteins, the domain is organized as a dual repeat of a helix−loop−helix motif, with a small β-sheet (residues 354−356 and 390−392) connecting the two ion-binding loops (Figure 4B). The helices are hereafter referred to as A, B, C, and D, with A/B in the first calcium-binding loop and C/D in the second, extending from 343 to 347, 357

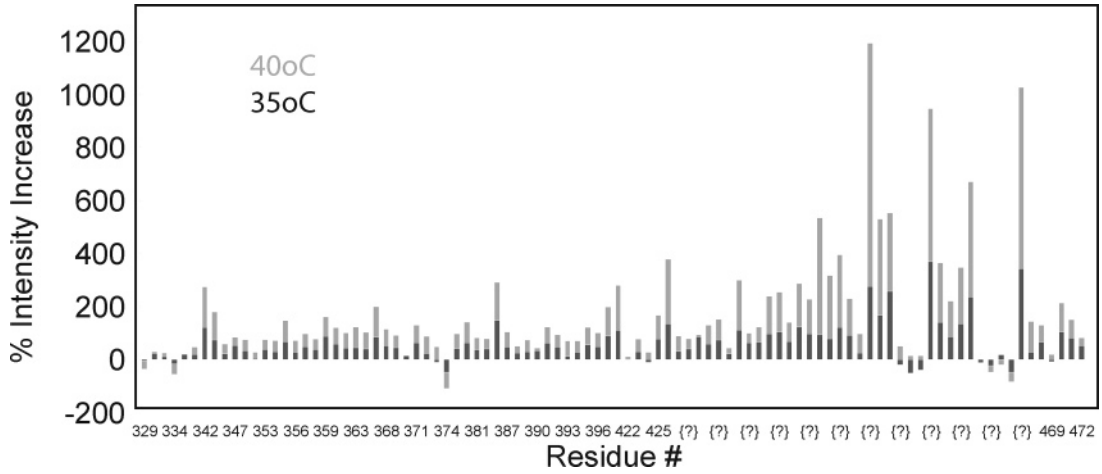

FIGURE 3: Comparison of percentage intensity increase at 35 and 40 °C in well-resolved $^{1}H,^{15}N$-HSQC peaks on increasing temperature as compared with a base intensity at 25 °C of NtH-CLD. The assigned residues from the N-terminal domain generally exhibit less dramatic intensity increases than unassigned peaks, which are presumably from the C-terminus (indicated by question marks).

Table 1: Statistics for the 15 Lowest Energy NtH-CLD Structures

rmsd from distance restraints (Å)	0.021 ± 0.002
rmsd from dihedral restraints (deg)	0.324 ± 0.082
deviations from idealized geometry	
bonds (Å)	0.002 ± 0.0001
angles (deg)	0.366 ± 0.018
impropers (deg)	0.282 ± 0.039
PROCHECK Ramachandran analysis (%)	
most favored regions	74.9
additional allowed regions	22.2
generously allowed regions	2.9
disallowed regions	0.1
van der Waals energy (kcal/mol)	74 ± 5
rmsd from lowest energy structure (Å)	
343−398 (well ordered)	
backbone	0.912
heavy	1.486
unambiguous restraints (total)	765
intraresidue	202
sequential	288
medium range	172
long range	103
ambiguous restraints (total)	118
dihedral restraints (ψ, ϕ)	130

Table 2: Interhelical Angles for CLD, CaM, and sTnC Structures

structure (PDB code)	helices A/B (deg)	helices C/D (deg)
NtH-CLD	83 ± 9	97 ± 8
JD-CLD	116 ± 4	103 ± 6
apo-CaM[a]	128 ± 2	130 ± 4
Ca^{2+}-CaM (NMR, 1J70)[b]	102 ± 1	100 ± 2
Ca^{2+}-CaM (X-ray, 1CLL)[c]	86	87
apo-sTnC (NMR, 1TNP)[d]	128 ± 3	125 ± 5
Ca^{2+}-sTnC (NMR, 1TNW)[e]	79 ± 3	78 ± 7

[a] From ref *49*. [b] From ref *42*. [c] From ref *41*. [d] From ref *50*. [e] From ref *51*.

to 365, 373 to 383, and 393 to 396, respectively. Interestingly, some structures in the ensemble have slightly extended A (toward the N-terminus) and/or D helices (toward the C-terminus), which is not altogether surprising considering that the consensus regions consist of only 1−1.5 turns (five and four residues, respectively). In both cases, chemical shift index data suggest that indeed the helices extend further than the calculated structures demonstrate (data not shown). Also common to both helices is evidence of significant exchange broadening in the $^{1}H,^{15}N$-HSQC of the residues where the helical regions break (i.e., 341 and 342 for A and 398 and 399 for D). Conformational exchange of these residues is corroborated by backbone relaxation data, as described later.

Interhelical contacts are observed between helices A/B, A/D, B/C, and C/D, as is seen with JD-CLD (*11*) and also CaM. Table 2 lists the interhelical angles of NtH-CLD, JD-CLD, apo-CaM, and Ca^{2+}-CaM [X-ray (*41*) and NMR (*42*)]. NtH-CLD demonstrates a relatively open conformation, with interhelical angles of 83 ± 9° for A/B and 97 ± 8° for C/D. (Note: the relatively large range is due to the short A and D helices, where slight differences in spatial position give rise to relatively large effects on the calculated angle.) The A/B angle is similar to that of the CaM crystal structure (86°) and more open than that of the NMR structure (102 ± 1°); the opposite is true for the C/D angle (X-ray, 87°; NMR, 100 ± 2°). Compared to skeletal muscle troponin C, another bilobal helix−loop−helix Ca^{2+}-binding protein, the A/B angle of NtH-CLD is very similar to sTnC (79 ± 3°), while the B/C loop is about 20° more closed than sTnC (78 ± 7°). Even more interesting is the comparison with the recently described JD-CLD complex. The C/D helical angles are well within the experimental uncertainty (JD-CLD, 103 ± 6°); however, there is a significant difference between the observed A/B helical orientations (JD-CLD, 116 ± 4°), with the complex structure being much more closed.

Backbone rmsd measurements further underscore the difference between the NtH-CLD structure and the N-terminal domain of JD-CLD. The rmsd between the well-ordered regions of NtH-CLD and JD-CLD is 3.16 Å, while between NtH-CLD and the Ca^{2+}-CaM crystal structure it is 2.32 Å. The rmsd between JD-CLD and Ca^{2+}-CaM is reasonably close at 2.26 Å, which is not altogether surprising based on the interhelical angles. An overlay of the backbone for CaM, NtH-CLD, and JD-CLD (Figure 4C) demonstrates that, as suggested by the helical angle and rmsd data, the conformation of Ca^{2+}-CaM in the crystal structure lies between a relatively open NtH-CLD and a closed JD-CLD.

Figure 4C presents a surface electric potential plot of the NtH-CLD structure. There is a large hydrophobic cleft comprised of residues L343, M346, I347, L360, L364, L379, Y393, F396, and I397. This pocket is more extensive than that found in the structure of JD-CLD and involves more residues from the N-terminal helix. This is explained by the

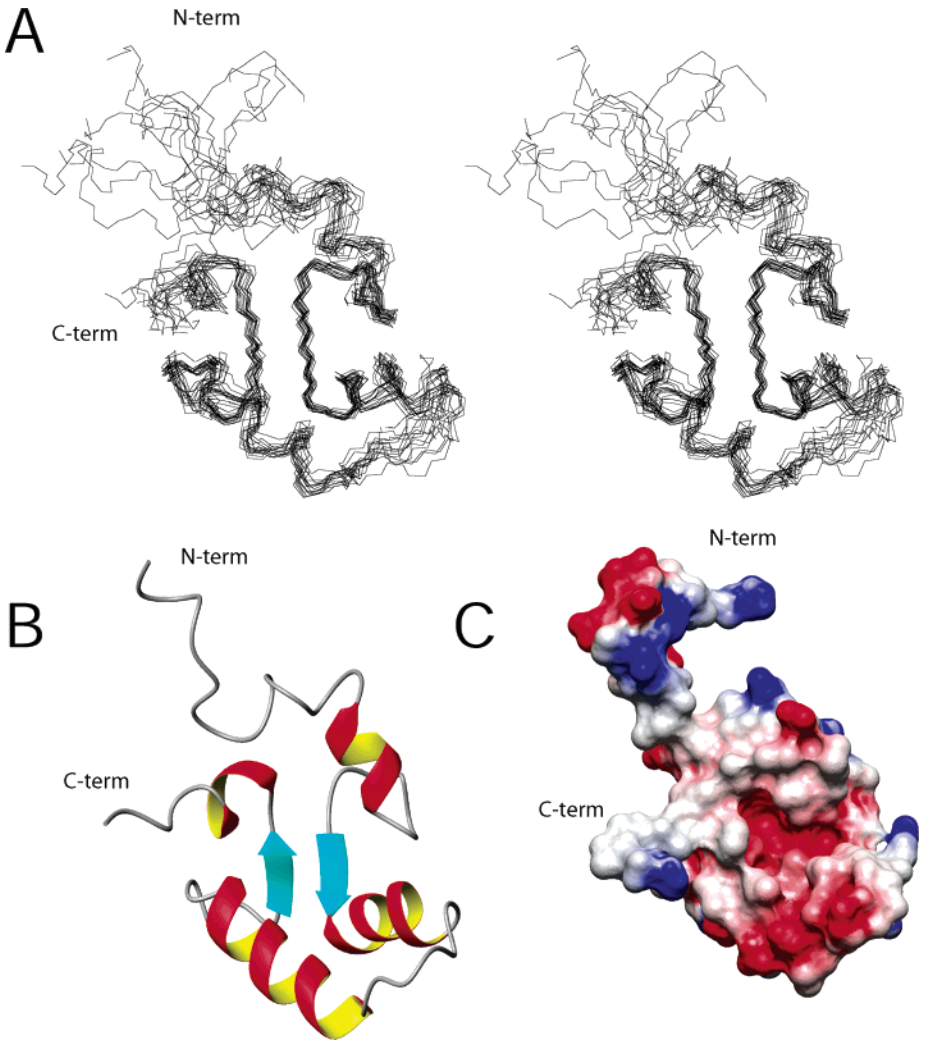

FIGURE 4: Structure of NtH-CLD displayed as a (A) stereoview backbone trace of the 15 lowest energy structures, (B) ribbon diagram of the lowest energy structure, and (C) electrostatic potential plot compared with Ca^{2+}-CaM (*41*), blue, and JD-CLD (*11*), green. All figures are in the same orientation. Note in (A) that the N-terminal region prior to the first helix, encompassing the tether region, is relatively disordered, although helical structure is evident in several structures for the first three residues and as an N-terminal extension to the first helix. In (C) negative charge areas are highlighted in red, positive in blue, and uncharged residues in white. Note the large pocket formed, the surface of which is lined by hydrophobic residues as outlined in the text. In (B) and (C) the fold is evidently very similar to JD-CLD and CaM; however, significant deviations are highlighted as the region between the two calcium-binding loops and helix D. The interhelical angle between the two helices in the first Ca^{2+} loop is on average >30° more open in the NtH-CLD structure as compared to the JD-CLD structure, giving rise to the observed differences. Figures created with MolMol (*52*).

fact that the NtH-CLD structure shows an A/B angle almost 30° more open. Similar to JD-CLD, there is a cluster of negatively charged residues on the opposite end to the tether region, consisting of E370, E375, and D378, and a number of negative charges below the hydrophobic cleft from residues involved in calcium binding. Interestingly, there is also a cluster of positive charges near the N-terminus, part of which comes from R331, and the rest from residues in the His tag.

Backbone Dynamics. To better understand the dynamic characteristics of NtH-CLD, ^{15}N relaxation parameters (T_1, T_2, and $\{^1H\}-^{15}N$ NOE) were obtained at 500 MHz ^1H frequency. Residues which could not be reliably fit due to overlap or poor signal to noise ratio were discarded, providing 55 residues in the CLD region of the construct. Most regions of the protein were well represented by the available data, although only residue 338 was available between 337 and 341 (Figure 5).

Initially, residues selected for determination of the τ_m were filtered by eliminating residues with ^{15}N NOE <0.65. This selection process eliminated residues 329, 330, 333, 334, 335, 336, 370, and 371. Structurally, these residues are located either in the unstructured N-terminal region or the loop between the two helix−loop−helix calcium-binding motifs. The remaining residues were used to calculate parameters for the initial estimate of the isotropic τ_m. All attempts to obtain an initial τ_m using the usual S^2 or $S^2-\tau_e$ model failed. This could be explained by the fact that the dominant exchange broadening observed in the nearby C-terminal is also present in the N-terminal domain, although to a lesser extent. Consequently, proper fit for the initial τ_m estimate could only be obtained by taking into account the effect of exchange broadening affecting the T_2 of most residues. Residues 348, 355, 365, 367, 369, and 399 did not fit well with the S^2-R_{ex} model and were not used for the initial τ_m estimate. The remaining 41 residues were therefore selected as good global representatives for the dynamics present in the N-terminal domain, and an initial τ_m of 9.84 ± 0.27 ns was obtained.

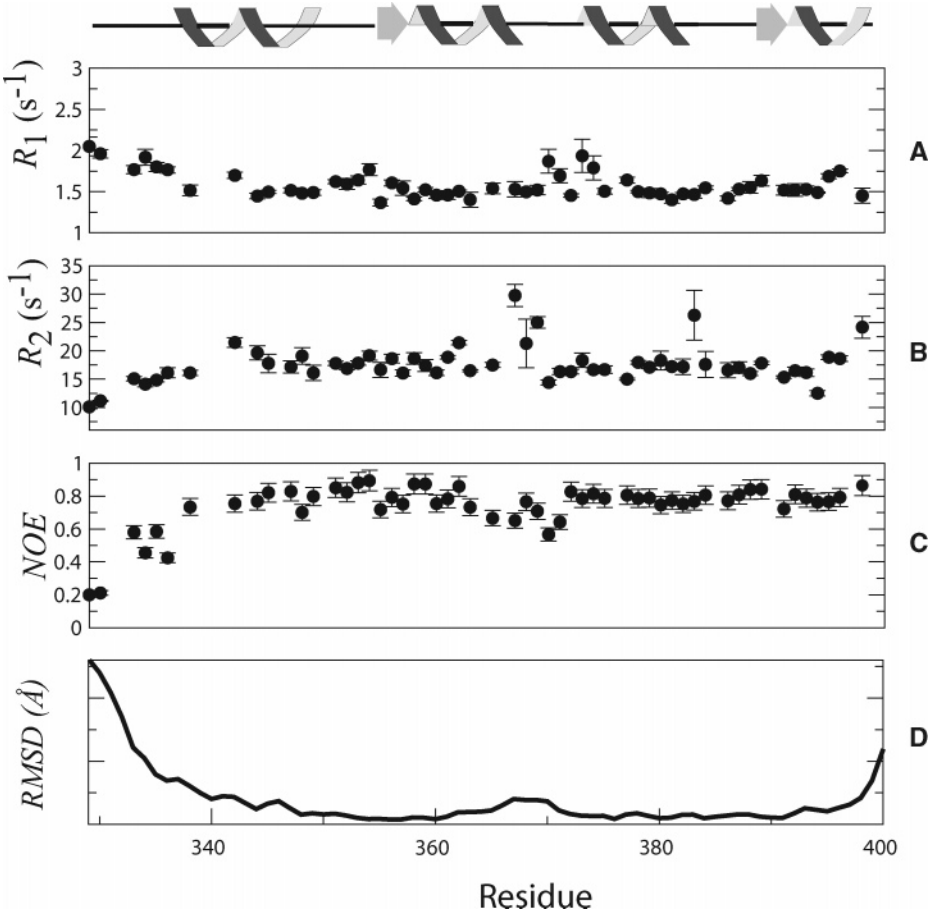

FIGURE 5: (A) ^{15}N R_1, (B) ^{15}N R_2, and (C) $\{^1H\}-^{15}N$ NOE relaxation data at 500 MHz ^1H frequency plotted as a function of residue number of NtH-CLD. Note that R_1 and R_2 are the reciprocals of T_1 and T_2, respectively. (D) Backbone rmsd values are for the entire ensemble of structures.

The relaxation data were used to calculate motional parameters for individual residues using the statistical model-free approach (*35*). The final correlation time for the domain once appropriate models were chosen for all residues was 8.06 ± 0.47 ns. Of the 58 residues that were fitted, 1 was best fitted with the $S^2-\tau_e$ model, 41 were best fitted with the S^2-R_{ex} model, 15 were best fitted with the $S^2-\tau_e-R_{ex}$ model, and 1 was best fitted with the two time scale model. Therefore, most residues could be fitted with a two-parameter model. Values obtained for S^2, τ_e, and R_{ex} are plotted in panels A−C of Figure 6, respectively. Generally, the data suggest fairly uniform movement of the entire domain with notable exceptions. It is readily apparent that much of the N-terminal tether region is highly mobile, up to and including the "extended" portions of helix A (from residues 335−342). This region shows that lower than average $\{^1H\}-^{15}N$ NOE values, higher than average internal motions (τ_e), and lower than average exchange terms (R_{ex}) were required for fitting. Also of note are lower than average $\{^1H\}-^{15}N$ NOE values of the linker region between helices B and C dividing the two Ca^{2+}-binding loops. This result suggests increased flexibility of this region, although the order parameters for residues 370, 373, and 374 are higher than average. This region also exhibits the highest exchange constant values, in particular residues 376−369, and interestingly, their line shapes in the $^1H-^{15}N$-HSQC were correspondingly exchange broadened as compared to other resonances. Significant exchange constants are observed for residue 398 at the termini of helix D, which in the determined structure of NtH-CLD is quite short (1−1.5 helical turns). Finally, significant exchange was evident for residue 383, at the end of helix C, which has been demonstrated to be important for interactions between the N- and C-domains of the CLD (*11*).

DISCUSSION

Global Motion versus Interdomain Movement. It is remarkable just how distinct the conformational behavior of the CLD from CDPK is from CaM, despite sharing >40% sequence identity and a common fold for both the N-terminal domain and C-terminal domain (*5*, *11*). On a global level, in the Ca^{2+} form, the rotational correlation time calculated in this study (~8 ns) is slightly larger than that expected if the N-terminal domain of the CLD was tumbling independently. For example, the correlation times for the two lobes of CaM are ~6−7 ns (*43*) when using a similar approach to that employed in this study, although this may be misleading due to the presence of slow interdomain motions (*44*).

Particularly intriguing is the exquisite equilibrium between the N-terminal and C-terminal domains and the roles that the JD and C-terminal tail might play in stabilizing this interaction. For example, the difference between the construct used in this study and that used for a complex with the JD and CLD (*11*) is an additional N-terminal His tag and the removal of the C-terminal tail in NtH-CLD (Figure 1C). The key Ca^{2+}-binding motifs, notably encompassing the entire region which is homologous to CaM, is conserved in both constructs, yet almost the entire C-terminal domain is broadened in the NMR spectra of NtH-CLD (Figure 3),

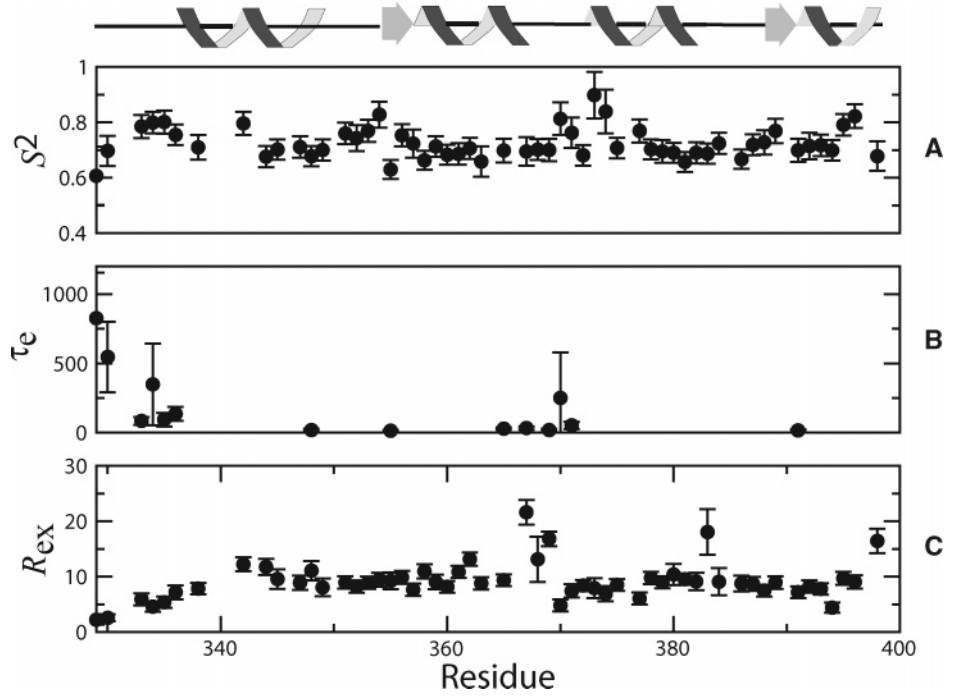

FIGURE 6: (A) Order parameters (S^2), (B) internal motions (τ_e), and (C) exchange constants (R_{ex}) obtained using the final τ_m of 8.06 ± 0.47 ns.

presumably by conformational exchange. It is worth noting that our previous work has shown that the JD-CLD interaction occurs primarily in the C-terminal domain, and hence this region may be sensitive to the presence of the N-terminal His tag in this study, which is in a homologous position to the JD in the intact CDPK.

The exact time scale of the interdomain motions presents a complicated question, especially in light of the numerous intradomain motions which are likely taking place concurrently. This presents an interesting situation, where the overall motion of the two domains is not necessarily independent. Complete analysis of this type of motion has been performed on other protein systems for more accurate quantification (*44*−*46*) and certainly represents another avenue for study. Nevertheless, we can speculate about the spatial nature of the interdomain motion. The JD-CLD structure demonstrates that helix C and helix E (from the C-terminal domain) interact (*11*). The unusual S^2 values observed for residues at the beginning of this helix, coupled with the significant exchange term for A383, indicate that there are some unusual dynamics, probably because A383 has been found to interact with the C-terminal domain (*11*). The extent of resonance broadening in A383 of NtH-CLD is significantly less than in JD-CLD, however, indicating that the interaction with the C-terminal domain is less pronounced or in a fast-exchange regime. This is consistent with the calculated correlation time of ~8 ns, which indicates that the N-terminal domain is relatively independent of the C-terminal domain in NtH-CLD.

Intradomain Exchange. The low $\{^1H\}-^{15}N$ NOE values observed for residues in the linker region between the two metal-binding motifs and at the beginning of helix C suggest that there are relatively large amplitude motions in this area, and it may be acting as a "hinge" in the intradomain motion of the N-terminal domain. This postulation is supported by the relatively high exchange terms in this region, as compared to the fairly homogeneous values through the rest of the protein.

Intradomain exchange is indicated not only by the R_{ex} terms in the dynamics data in all areas of the structure (i.e., not only those areas which could be interacting with the C-terminal domain) but also by the difference in the interhelical angles between NtH-CLD and JD-CLD. The difference between the A/B helices in the two structures is surprisingly >30°, with the NtH-CLD structure being more open. Moreover, a noteworthy interaction in this context is observed for NtH-CLD between G338 and Y393. G338 is the first of two Gly residues at the interface between the "tether region" at the immediate N-terminus of the CLD and the remainder of the Ca^{2+}-binding region. This interaction is not observed in the JD-CLD structure as the resonances for G338 and G339 are not observed due to exchange broadening. This result may be a consequence of having residues appended N-terminal to the CLD (in this case the His tag used for purification), which were not present in the JD-CLD study.

Nevertheless, it is clear that some factor, whether it be the presence of the JD in JD-CLD or the additional N-terminal residues in NtH-CLD, causes a significant change. It has been suggested that CaM's ability to bind multiple targets has some origin in the plasticity of the N-terminal domain as evidenced by different interhelical angles in the Ca^{2+} form as derived by NMR (*42*) and X-ray crystallography (*41*). We speculate that a similar "scissoring" motion may be involved in binding of the JD. Several biochemical studies have been carried out to characterize the interaction between the JD and CLD (for example, refs *8* and *9*), and consistently, the enzyme activity of intact CDPK is significantly greater than activity derived from bimolecular reconstitution using exogenous CLD. Our results suggest that this may be the result of a significant conformational change in the A helix of CLD. Qualitatively, the line broadening of the peaks in NtH-CLD, especially in helices A and D, is much less evident in the N-terminal domain than that seen for JD-CLD, suggesting that either

the movement of the NtH-CLD is in a faster exchange regime or the motions are restricted to a more limited range of residues as indicated by the R_{ex} fitting of the dynamics data (Figure 6).

The Tether Region. A major advantage of studying NtH-CLD over the JD-CLD construct is the ability to examine the behavior of the tether region (*10*). This region consists of the first 11 residues of CLD (A329−G340) and has been found to be critical in intramolecular binding of the CLD to the JD, yet is completely exchange broadened in JD-CLD. In the structures calculated in this study, the first three residues are consistently structured in a helical turn with the last two residues of the N-terminal His tag, consistent with observed d_{NN} NOE's. It is not clear if this represents innate helical character of this region, which would be attached to the CaM-binding region of the JD in intact CDPK, or an artifact of the His tag. Recent chemical shift data from *Arabidopsis* CDPK isoform CPK-1 suggests that the JD is helical when attached to the CLD (*47*), and the helical bend of the initial part of the tether region may well be innate. Subsequently, there is a clear break in the helix, with a series of strong $d_{\alpha N}$ NOE's between residues 332−335, characteristic of β-structure (*48*). This is quite intriguing, as it establishes a defined structural means by which the JD may be sterically positioned with respect to the CLD. Overall, this region appears to be quite mobile and undergoing conformation exchange as indicated by the low S^2 values and R_{ex} terms, and it may be a combination of high mobility and break in the helical structure between the JD and helix A of the CLD which renders the tether region sensitive to intramolecular activation of CDPK.

This work has specifically examined the Ca^{2+} form of the CLD, and while the construct used in this study is different from previous structural work done with soybean CDPK-α CLD, it is intriguing to note that, in all cases, the C-terminal domain appears to be more conformationally variable than the N-terminal domain. For example, chemical shift mapping studies (*11*) specifically demonstrate that there is a significant change in the C-terminal lobe between the Ca^{2+}-CLD and Ca^{2+}-JD-CLD construct (i.e., Figure 1C with and without the JD peptide). In the current study, the C-terminal domain is essentially not NMR visible, due to conformational exchange, highlighting the importance of this domain. It is not clear if the invisibility of the C-terminal domain, in particular the fourth Ca^{2+}-binding region, is due to partial unfolding and/or a very weak calcium binding in NtH-CLD, or some other phenomena, and is certainly an avenue for further investigation. Combined with other data which provide information about the global changes associated with Ca^{2+} binding and interaction of the CLD with the JD (*13*, *14*), it is tempting to suggest that the conformational exchange observed, and in particular the positioning of the two domains, is important for the fine-tuned functioning of the CLD.

REFERENCES

1. Sanders, D., Pelloux, J., Brownlee, C., and Harper, J. F. (2002) Calcium at the crossroads of signaling, *Plant Cell 14* (Suppl.), S401−S417.
2. Harper, J. F., Sussman, M. R., Schaller, G. E., Putnam-Evans, C., Charbonneau, H., and Harmon, A. C. (1991) A calcium-dependent protein kinase with a regulatory domain similar to calmodulin, *Science 252*, 951−954.
3. Harmon, A. C., Gribskov, M., and Harper, J. F. (2000) CDPKs—a kinase for every Ca2+ signal?, *Trends Plant Sci. 5*, 154−159.
4. Cheng, S. H., Willmann, M. R., Chen, H. C., and Sheen, J. (2002) Calcium signaling through protein kinases. The *Arabidopsis* calcium-dependent protein kinase gene family, *Plant Physiol. 129*, 469−485.
5. Weljie, A. M., Clarke, T. E., Juffer, A. H., Harmon, A. C., and Vogel, H. J. (2000) Comparative modeling studies of the calmodulin-like domain of calcium-dependent protein kinase from soybean, *Proteins 39*, 343−357.
6. Harmon, A. C., Yoo, B. C., and McCaffery, C. (1994) Pseudosubstrate inhibition of CDPK, a protein kinase with a calmodulin-like domain, *Biochemistry 33*, 7278−7287.
7. Harper, J. F., Huang, J. F., and Lloyd, S. J. (1994) Genetic identification of an autoinhibitor in CDPK, a protein kinase with a calmodulin-like domain, *Biochemistry 33*, 7267−7277.
8. Yoo, B. C., and Harmon, A. C. (1996) Intramolecular binding contributes to the activation of CDPK, a protein kinase with a calmodulin-like domain, *Biochemistry 35*, 12029−12037.
9. Huang, J. F., Teyton, L., and Harper, J. F. (1996) Activation of a Ca(2+)-dependent protein kinase involves intramolecular binding of a calmodulin-like regulatory domain, *Biochemistry 35*, 13222−13230.
10. Vitart, V. V., Christodoulou, J., Huang, J. F., Chazin, W. J., and Harper, J. F. (2000) Intramolecular activation of a Ca(2+)-dependent protein kinase is disrupted by insertions in the tether that connects the calmodulin-like domain to the kinase, *Biochemistry 39*, 4006−4011.
11. Weljie, A. M., and Vogel, H. J. (2004) Unexpected structure of the Ca2+-regulatory region from soybean calcium-dependent protein kinase-alpha, *J. Biol. Chem. 279*, 35494−35502.
12. Zhao, Y., Pokutta, S., Maurer, P., Lindt, M., Franklin, R. M., and Kappes, B. (1994) Calcium-binding properties of a calcium-dependent protein kinase from *Plasmodium falciparum* and the significance of individual calcium-binding sites for kinase activation, *Biochemistry 33*, 3714−3721.
13. Weljie, A. M., Yamniuk, A. P., Yoshino, H., Izumi, Y., and Vogel, H. J. (2003) Protein conformational changes studied by diffusion NMR spectroscopy: application to helix-loop-helix calcium binding proteins, *Protein Sci. 12*, 228−236.
14. Weljie, A. M., Robertson, K. M., and Vogel, H. J. (2003) Conformational changes in the Ca2+-regulatory region from soybean calcium-dependent protein kinase-alpha: fluorescence resonance energy transfer studies, *J. Biol. Chem. 278*, 43764−43769.
15. Kohno, T., Kusunoki, H., Sato, K., and Wakamatsu, K. (1998) A new general method for the biosynthesis of stable isotope-enriched peptides using a decahistidine-tagged ubiquitin fusion system: an application to the production of mastoparan-X uniformly enriched with ^{15}N and $^{15}N/^{13}C$, *J. Biomol. NMR 12*, 109−121.
16. Muhandiram, D. R., and Kay, L. E. (1994) Gradient-enhanced triple resonance three-dimensional NMR experiments with improved sensitivity, *J. Magn. Reson. B 103*, 203−216.
17. Grzesiek, S., and Bax, A. (1992) Improved 3D triple-resonance NMR techniques applied to a 31-KDa protein, *J. Magn. Reson. 96*, 432−440.
18. Wittekind, M., and Mueller, L. (1993) HNCACB, a high sensitivity 3D NMR experiment to correlate H(N) AND 15N resonances with the alpha-carbon and beta-carbon resonances in proteins, *J. Magn. Reson. B 101*, 201−205.
19. Clubb, R. T., Thanabal, V., and Wagner, G. (1992) A constant-time 3-dimensional triple-resonance pulse scheme to correlate intraresidue H-1(N), N-15, and C-13(′) chemical-shifts in N-15-C-13-labeled proteins, *J. Magn. Reson. 97*, 213−217.
20. Marion, D., Driscoll, P. C., Kay, L. E., Wingfield, P. T., Bax, A., Gronenborn, A. M., and Clore, G. M. (1989) Overcoming the overlap problem in the assignment of ^1H NMR spectra of larger proteins by use of three-dimensional heteronuclear ^1H-^{15}N Hartmann−Hahn-multiple quantum coherence and nuclear Overhauser-multiple quantum coherence spectroscopy: application to interleukin 1 beta, *Biochemistry 28*, 6150−6156.
21. Montelione, G. T., Lyons, B. A., Emerson, S. D., and Tashiro, M. (1992) An efficient triple resonance experiment using C-13 isotropic mixing for determining sequence-specific resonance assignments of isotopically-enriched proteins, *J. Am. Chem. Soc. 114*, 10974−10975.
22. Bax, A., and Grzesiek, S. (1993) Methodolgical advances in protein NMR, *Acc. Chem. Res. 26*, 131−138.

23. Markley, J. L., Bax, A., Arata, Y., Hilbers, C. W., Kaptein, R., Sykes, B. D., Wright, P. E., and Wuthrich, K. (1998) Recommendations for the presentation of NMR structures of proteins and nucleic acids. IUPAC−IUBMB−IUPAB inter-union task group on the standardization of data bases of protein and nucleic acid structures determined by NMR spectroscopy, *J. Biomol. NMR 12*, 1−23.
24. Delaglio, F., Grzesiek, S., Vuister, G. W., Zhu, G., Pfeifer, J., and Bax, A. (1995) NMRPipe: a multidimensional spectral processing system based on UNIX pipes, *J. Biomol. NMR 6*, 277−293.
25. Johnson, B. A., and Blevins, R. A. (1994) NMRView: A computer program for the visualization and analysis of NMR data, *J. Biomol. NMR 4*, 603−614.
26. Brunger, A. T., Adams, P. D., Clore, G. M., DeLano, W. L., Gros, P., Grosse-Kunstleve, R. W., Jiang, J. S., Kuszewski, J., Nilges, M., Pannu, N. S., Read, R. J., Rice, L. M., Simonson, T., and Warren, G. L. (1998) Crystallography & NMR system: A new software suite for macromolecular structure determination, *Acta Crystallogr., Sect. D: Biol. Crystallogr. 54* (Part 5), 905−921.
27. Nilges, M., and O'Donoghue, S. I. (1998) Ambiguous NOEs and automated NOESY assignment, *Prog. NMR Spectrosc. 32*, 107−139.
28. Wishart, D. S., and Nip, A. M. (1998) Protein chemical shift analysis: a practical guide, *Biochem. Cell Biol. 76*, 153−163.
29. Cornilescu, G., Delaglio, F., and Bax, A. (1999) Protein backbone angle restraints from searching a database for chemical shift and sequence homology, *J. Biomol. NMR 13*, 289−302.
30. Marsden, B. J., Shaw, G. S., and Sykes, B. D. (1990) Calcium binding proteins. Elucidating the contributions to calcium affinity from an analysis of species variants and peptide fragments, *Biochem. Cell Biol. 68*, 587−601.
31. Laskowski, R. A., Rullman, J. A. C., MacArthur, M. W., Kaptein, R., and Thornton, J. M. (1996) AQUA and PROCHECK-NMR: Programs for checking the quality of protein structures solved by NMR, *J. Biomol. NMR 8*, 477−486.
32. Farrow, N. A., Muhandiram, R., Singer, A. U., Pascal, S. M., Kay, C. M., Gish, G., Shoelson, S. E., Pawson, T., Forman-Kay, J. D., and Kay, L. E. (1994) Backbone dynamics of a free and phosphopeptide-complexed Src homology 2 domain studied by ^{15}N NMR relaxation, *Biochemistry 33*, 5984−6003.
33. Grzesiek, S., and Bax, A. (1993) The importance of not saturating H_2O in protein NMR: Application to sensitivity enhancement and NOE measurements, *J. Am. Chem. Soc. 115*, 12593−12594.
34. Viles, J. H., Duggan, B. M., Zaborowski, E., Schwarzinger, S., Huntley, J. J., Kroon, G. J., Dyson, H. J., and Wright, P. E. (2001) Potential bias in NMR relaxation data introduced by peak intensity analysis and curve fitting methods, *J. Biomol. NMR 21*, 1−9.
35. Mandel, A. M., Akke, M., and Palmer, A. G., III (1995) Backbone dynamics of *Escherichia coli* ribonuclease HI: correlations with structure and function in an active enzyme, *J. Mol. Biol. 246*, 144−163.
36. Palmer, A. G., Rance, M., and Wright, P. E. (1991) Intramolecular motions of a zinc finger DNA-binding domain from Xfin characterized by proton-detected natural abundance C-12 heteronuclear NMR spectroscopy, *J. Am. Chem. Soc. 113*, 4371−4380.
37. Tjandra, N., Feller, S. E., Pastor, R. W., and Bax, A. (1995) Rotational diffusion anisotropy of human ubiquitin from ^{15}N NMR relaxation, *J. Am. Chem. Soc. 117*, 12562−12566.
38. Lipari, G., and Szabo, A. (1982) Model-free approach to the interpretation of nuclear magnetic resonance relaxation in macromolecules. 1. Theory and range of validity, *J. Am. Chem. Soc. 104*, 4546−4559.
39. Lipari, G., and Szabo, A. (1982) Model-free approach to the interpretation of nuclear magnetic resonance relaxation in macromolecules. 2. Analysis of experiemental results, *J. Am. Chem. Soc. 104*, 4559−4570.
40. Wishart, D. S., Sykes, B. D., and Richards, F. M. (1991) Relationship between nuclear magnetic resonance chemical shift and protein secondary structure, *J. Mol. Biol. 222*, 311−333.
41. Chattopadhyaya, R., Meador, W. E., Means, A. R., and Quiocho, F. A. (1992) Calmodulin structure refined at 1.7 Å resolution, *J. Mol. Biol. 228*, 1177−1192.
42. Chou, J. J., Li, S., Klee, C. B., and Bax, A. (2001) Solution structure of Ca(2+)-calmodulin reveals flexible hand-like properties of its domains, *Nat. Struct. Biol. 8*, 990−997.
43. Barbato, G., Ikura, M., Kay, L. E., Pastor, R. W., and Bax, A. (1992) Backbone dynamics of calmodulin studied by ^{15}N relaxation using inverse detected two-dimensional NMR spectroscopy: the central helix is flexible, *Biochemistry 31*, 5269−5278.
44. Baber, J. L., Szabo, A., and Tjandra, N. (2001) Analysis of slow interdomain motion of macromolecules using NMR relaxation data, *J. Am. Chem. Soc. 123*, 3953−3959.
45. Korzhnev, D. M., Orekhov, V. Y., and Arseniev, A. S. (1997) Model-free approach beyond the borders of its applicability, *J. Magn. Reson. 127*, 184−191.
46. Chang, S. L., and Tjandra, N. (2001) Analysis of NMR relaxation data of biomolecules with slow domain motions using wobble-in-a-cone approximation, *J. Am. Chem. Soc. 123*, 11484−11485.
47. Christodoulou, J., Hu, H., Chung, J., Rance, M., Harper, J. F., and Chazin, W. J. (2002) Letter to the Editor: ^{1}H, ^{15}N, and ^{13}C assignments of the regulatory domains of calcium-dependent protein kinase (CDPK), *J. Biomol. NMR 23*, 249−250.
48. Wuthrich, K. (1986) *NMR of Proteins and Nucleic Acids*, John Wiley & Sons, New York.
49. Zhang, M., Tanaka, T., and Ikura, M. (1995) Calcium-induced conformational transition revealed by the solution structure of apo calmodulin, *Nat. Struct. Biol. 2*, 758−767.
50. Gagne, S. M., Tsuda, S., Li, M. X., Smillie, L. B., and Sykes, B. D. (1995) Structures of the troponin C regulatory domains in the apo and calcium-saturated states, *Nat. Struct. Biol. 2*, 784−789.
51. Slupsky, C. M., and Sykes, B. D. (1995) NMR solution structure of calcium-saturated skeletal muscle troponin C, *Biochemistry 34*, 15953−15964.
52. Koradi, R., Billeter, M., and Wuthrich, K. (1996) MOLMOL: a program for display and analysis of macromolecular structures, *J. Mol. Graphics 14*, 51−32.

BI048751R